# A GENERAL APPROACH TO THE GEOSTATIONARY TRANSFER ORBIT MISSION RECOVERY

Nicolas Faber[1,2], Andrea Aresini[1], Pascal Wauthier[1] and Philippe Francken[1]

[1] SES Astra S.A., L-6815 Château de Betzdorf, Grand-Duchy of Luxembourg
[2] Observatory of Strasbourg, 11 rue de l'Observatoire, 67000 Strasbourg, France

***Abstract:*** *This paper discusses recovery scenarios for geosynchronous satellites injected in a non-nominal orbit due to a launcher underperformance. The theory on minimum-fuel orbital transfers is applied to develop an operational tool capable to design a recovery mission. To obtain promising initial guesses for the recovery three complementary techniques are used: p-optimized impulse function contouring, a numerical impulse function minimization and the solutions to the switching equations. The tool evaluates the feasibility of a recovery with the on-board propellant of the spacecraft and performs the complete mission design. This design takes into account for various mission operational constraints such as e.g., the requirement of multiple finite-duration burns, third-body orbital perturbations, spacecraft attitude constraints and ground station visibility. In a final case study, we analyze the consequences of a premature breakdown of an upper rocket stage engine during injection on a geostationary transfer orbit, as well as the possible recovery solution with the satellite on-board propellant.*

## Abbreviations and Symbols

| | | |
|---|---|---|
| *GEO* | = | geosynchronous orbit |
| *GTO* | = | geostationary transfer orbit |
| *LAE* | = | satellite 'liquid apogee engine' |
| $j$ | = | index for infinite-thrust impulse $j$ ($j = 1, 2$) |
| $k$ | = | index for orbit specification ($1$ = initial orbit, $t$ = transfer orbit, $2$ = GEO) |
| $O_k$ | = | initial orbit, final orbit, transfer orbit (k = $1, 2, t$) |
| $a_k$, $e_k$, $i_k$, $\Omega_k$, $\omega_k$, $v_k$ | = | semi-major axis , eccentricity, inclination, right ascension of ascending node, argument of perigee, mean anomaly |
| $\theta_1$ | = | true anomaly of first impulse in initial orbit |
| $f_j$ | = | true anomaly of impulse $j$ in transfer orbit |
| $\Delta$ | = | transfer angle = $f_2 - f_1$ |
| $p_k$ | = | semi-latus rectum |
| $\boldsymbol{\Delta V}_j$ | = | thrust vector of impulse $j$ |
| $\Delta V_j$, $\Delta V_{tot}$ | = | velocity increment of impulse $j$, total velocity increment |
| $I_j$ | = | position of impulse $j$ |
| $\boldsymbol{R}_j$ | = | position vector of impulse $j$ |
| ($C$, $\boldsymbol{\gamma}$, $\boldsymbol{L}$, $\boldsymbol{North}$) | = | orthogonal 'Earth-centered inertial' coordinate system |
| ($C$, $\boldsymbol{x}$, $\boldsymbol{y}$, $\boldsymbol{z}$) | = | unit vectors in the 'Earth-centered inertial' system |
| $\alpha_i$, $\delta_j$ | = | right ascension and declination of impulse $j$ |
| ($M$, $\boldsymbol{S}$, $\boldsymbol{T}$, $\boldsymbol{W}$) | = | orthogonal 'radial-tangential-normal' coordinate system |

| | | |
|---|---|---|
| $\boldsymbol{X}$ | = | vector of unknowns ($\theta_1$, $\alpha_2$, $p_t$) |
| $S_j$, $T_j$, $W_j$ | = | components of the primer vector $\boldsymbol{P}_j$ |
| $\boldsymbol{w}$ | = | pole vector of transfer orbit |
| $\mu$ | = | gravitational constant |
| $\phi_j$ | = | sun angle for impulse $j$ |
| $a_{geo}$ | = | geostationary altitude (42164.170 km) |
| $I_{sp}$ | = | specific impulse of satellite *LAE* |
| $F$ | = | thrust of satellite *LAE* |

## I Introduction

A geostationary transfer orbit (hereafter *GTO*) mission encompasses the transfer of a satellite from a given injection orbit to geosynchronous orbit (hereafter *GEO*). Classical *GTO* mission designs rely on the insertion of the spacecraft by the launcher vehicle onto a target injection orbit. However, in the unlikely case of a non-nominal performance of the launcher, the GTO mission has to be re-designed considering new conditions. For example, in the case of a launch vehicle without re-ignitable engine, pointing errors may introduce considerable discrepancies between the parameters of the obtained injection orbit and the nominal one. Re-ignitable launchers, on the other hand, may suffer from a premature firing abort, possibly leading to an unexpected injection orbit such as an important misalignment of the line of nodes from the line of apses.
In the present contribution, we discuss such cases of launcher misbehavior for typically inclined *GTO* missions. We show how to compensate for a potential shortage of the launch vehicle whenever possible, by efficiently using the separated spacecraft on-board propellant to reach *GEO*. This compensation is performed by making use of the extensive amount of literature available on the general case of minimum-fuel transfers between two inclined elliptical orbits such as e.g., [1], [2], [3], [4], [5], [6], [7], [8], [9], [10], [11]. Whereas these contributions are carried out in the unrealistic limit of two infinite-thrust impulses applied in a Keplerian gravitational field, we propose in this paper to relax these approximations and to develop a realistic mission operational tool. This tool takes into account for all practical *GTO* mission operational constraints and evaluates the possibility of recovery for any non-nominal injection. Section II presents a general picture of the transfer geometry and introduces the variables used in the study. Section III summarizes our methodology and in Section IV we apply the technique to a test case, where we study the consequences of a premature abort of an upper rocket stage engine. Conclusions are presented in Section V.

## II Transfer Geometry

Let us consider the general case of a time-free, infinite-thrust transfer performed in a Keplerian (two-body) gravitational field. The transfer is performed between a known initial elliptical injection orbit $O_1$ and a final circular geostationary target orbit $O_2$, as described in Fig. 1. The classical Keplerian elements of these orbits are

$$O_1 = (a_1, e_1, i_1, \Omega_1, \omega_1, \theta_1) \quad (1)$$

for the initial orbit, and

$$O_2 = (a_2 = a_{geo}, e_2 = 0°, i_2 = 0°) \quad (2)$$

for the target orbit with $a_{geo}$ = 42164.170 km. These two orbits are connected by the transfer orbit $O_t$,

$$O_t = (a_t, e_t, i_t, \Omega_t, \omega_t, f_j) \quad (3)$$

through the application of the two impulses $\boldsymbol{\Delta V}_j$ at the impulse points $I_j$ with true anomalies $f_j$ ($j$ = 1, 2).

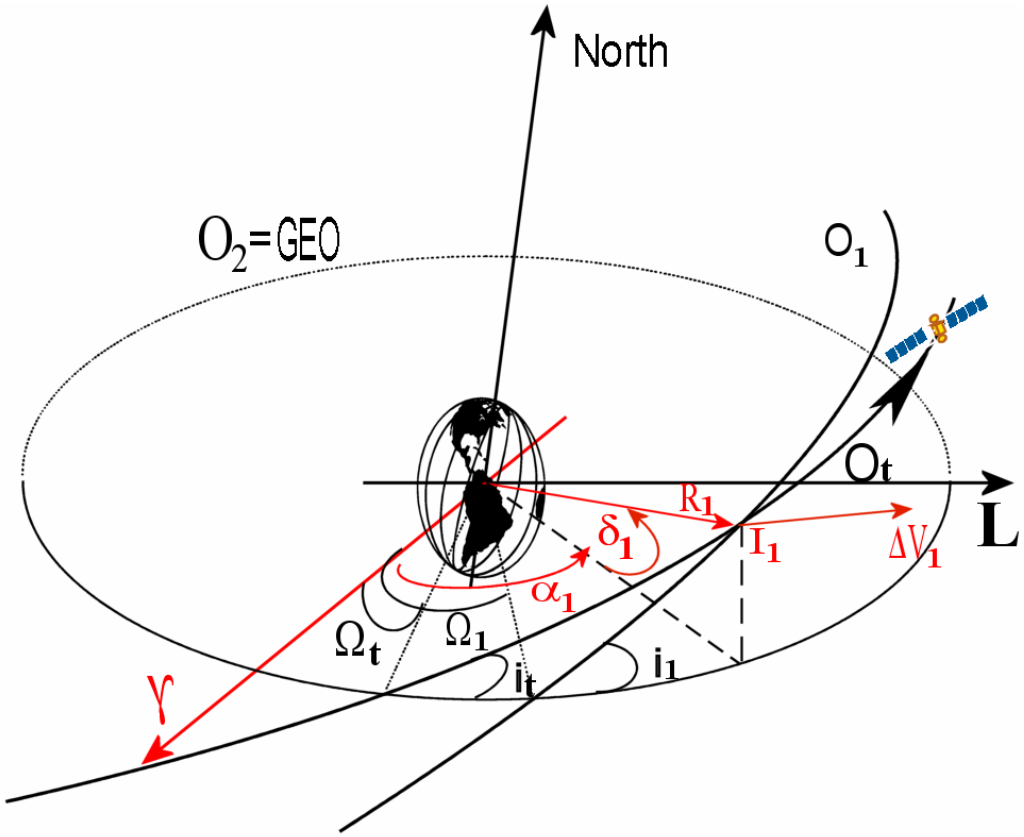


**Figure 1: General transfer geometry.**

The transfer is described by the means of two coordinate systems. First, the inertial system (C, ***γ***, ***L***, ***North***) is used, centered at the center of the Earth *C* (Fig. 1). For the sake of clarity, the corresponding system of unit vectors (*C*, ***x***, ***y***, ***z***) is not shown in Fig. 1. The spacecraft and the impulse points $I_j$ can now be located in inertial space in terms of their right ascensions $\alpha_j$ and declinations $\delta_j$ ($j$ = 1, 2). Along the transfer ellipse $O_t$, we also express the two impulses $\boldsymbol{\Delta V}_j$ in the rotating coordinate system (*M*, ***S***, ***T***, ***W***) as shown in Fig. 2. Here *M* is at the origin of the vehicle and ***S*** points along the direction of the position vector **R**, positive outwards. The vector ***T*** describes the circumferential direction of the satellite in the plane of $O_t$ and ***W*** complements the right-handed system.

## III Method

The goal is to design a recovery mission in the case of a non-nominal injection of the spacecraft. We define an injection to be non-nominal (or non-optimal) if at least one of the following two complications is encountered. First, the problem of a significant underperformance of the launch vehicle may occur. We define this to be the case whenever the semi-major axis $a_1$ of the injection orbit $O_1$ differs from its nominal value by more than a 3-sigma standard deviation. Second, one may have to deal with the situation where the node shift $\omega_1$ is such that the Simplified Nodal Transfer (SNT) strategy (see e.g., **[9], [12], [13]**) is far from optimum and thus not applicable. We define this to be the case whenever $\omega_1 > 20°$. The remaining injection orbit parameters $e_1$, $i_1$ and $\Omega_1$ are free parameters of the study.

The method has two main steps:

- Step 1: search for recovery scenarios to be used as initial guesses for Step 2 (see Section III.1)
- Step 2: practical development of a realistic and complete recovery mission design (see Section III.2)

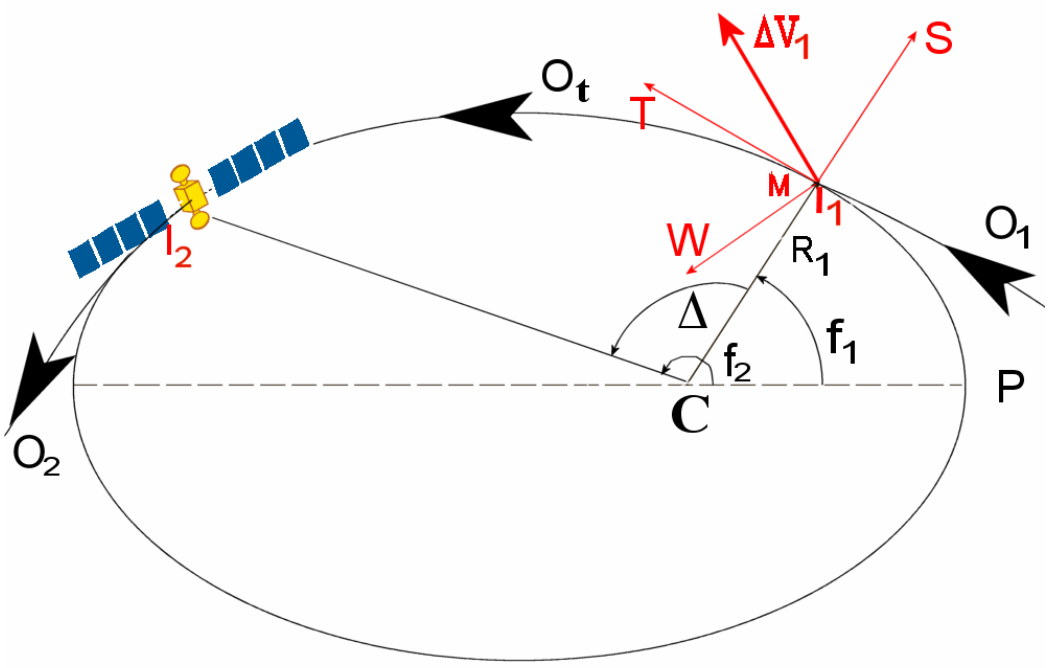


**Figure 2: Transfer orbit geometry**

### III.1 Step 1: Search for recovery scenarios

Following three complementary methods are used as a part of the first step: (1) p-optimized impulse function contouring (see Section III.1.1), (2) a numerical impulse function minimization (see Section III.1.2) and (3) the solutions to the switching equations (see Section III.1.3). These methods search for minimum-fuel solutions to perform the transfer to *GEO* and then evaluate the feasibility of a mission recovery with the on-board propellant of the spacecraft. The search is simplified by following two assumptions. First, the methods suppose that the transfer is realized by two infinite-thrust impulses. Second, they assume that the motion be entirely Keplerian i.e. Earth gravity and third-body orbital perturbations are neglected. Under these assumptions, the general problem of a minimum-fuel open-time transfer between two elliptical orbits comprises 8 control parameters (see e.g., **[1], [6]**). These are the 6 $\boldsymbol{\Delta V}_j$ impulse components and the 2 true anomalies $f_j$ of the impulses in the transfer orbit ($j$ = 1, 2). We have 5 constraints on the final orbit, namely $a_2$, $e_2$, $i_2$, $\Omega_2$, $\omega_2$. In consequence, there are 3 remaining free parameters left for the optimization of the total propellant expenditure (see e.g., **[2], [6], [8], [9]**)

$$\Delta V_{tot} = |\boldsymbol{\Delta V_1}| + |\boldsymbol{\Delta V_2}| \ . \tag{4}$$

The choice of these independent variables is determined by the optimization method one aims to implement. In this work we determine minimum $\Delta V_{tot}$ transfers by using the unknowns

$$\boldsymbol{X} = \begin{pmatrix} \theta_1 \\ \alpha_2 \\ p_t \end{pmatrix}, \tag{5}$$

where $\theta_1$ is the true anomaly of the first impulse in the injection orbit, $\alpha_2$ is the right ascension of the second impulse on *GEO* and $p_t$ is the parameter of the transfer orbit. These variables simplify the structure of the impulse function of Eq. (4) and avoid several undesirable discontinuities that are present in other formulations (see e.g., **[2]**).

*III.1.1 P-optimization of the impulse function*

We examine the behavior of the impulse function $\Delta V_{tot}$ by using a technique introduced by McCue **[2]**. The method consists in computing the magnitude of the total velocity increment as a function of the right ascensions $\alpha_1$ and $\alpha_2$ of the two impulses. A minimization of $\Delta V_{tot}$ for each couple ($\alpha_1$, $\alpha_2$) is then performed with respect to the third variable $p_t$, by implementing the so-called p-optimization technique. It is straightforward to obtain $\alpha_1$ by using the elements of $O_1$ (Eq. [1]) in conjunction with the true anomaly $\theta_1$ given by Eq. (5). The contour-map of the impulse function is then computed by using the unknowns ($\alpha_1$, $\alpha_2$, $p_t$). We refer to **[2]** for a complete formulation of the approach. For an explicit statement of the impulse function we refer to Section III.1.2, where $\Delta V_{tot}$ is computed in a slightly different manner as in **[2]**.
Figures 3-8 show the shape of the impulse function for a set of different injection orbits $O_1$. Figure 3 shows the $\Delta V_{tot}$ needed for the geostationary transfer in the case of an injection orbit $p_1$= 22000 km, $e_1$ = 0°, $i_1$= 0°, $\Omega_1$ = 0°, $\omega_1$ = 0°. The contour lines agree with the result obtained in Figure 3(a) of **[2]**. A symmetry about the $\alpha_1 - \alpha_2 = 0°$ plane is apparent and the Hohmann transfer would correspond to the straight line ($\alpha_1$, $\alpha_1$ + 180°, $p_t$) with an optimal $p_t$ of about 29000 km. We note that the method encounters a singularity when the transfer angle $\Delta \equiv 180°$, calling for a different approach. Throughout Figs. 4-8 we introduce eccentricity, inclination and node shift to the orbital elements of $O_1$. We recover the well-known shape of the impulse function for each of these initial configurations. For instance, artifacts such as the appearance of an 'inclination wall' are clearly recognizable in Figs. 5-8 and agree with the shape of the contours obtained in Figure 11 of **[2]**.

*III.1.2 Numerical minimization of the impulse function*

The p-optimized contour plots described in Section III.1.1 allow to visualize the shape of the impulse function $\Delta V_{tot}$ of Eq. (4) for a given injection orbit. However, no accurate recovery scenario can be derived from this technique since the result is only optimized with respect to one variable, namely $p_t$. In this section we propose to numerically optimize the transfer with respect to the three variables $\boldsymbol{X}(\theta_1, \alpha_2, p_t)$ (see Eq. [5]). We compute the transfer orbit parameters and derive an explicit form of the impulse function with respect to $\boldsymbol{X}$ by simple geometric arguments (**[14]**).
The radius of the first impulse can be written as

$$R_1 = \frac{a_1(1-e_1^2)}{(1+e_1 \cdot \cos\theta_1)} \tag{6}$$

and the corresponding position vector is

$$\boldsymbol{R_1} = \begin{pmatrix} R_1 \cdot [\cos\Omega_1 \cdot \cos(\omega_1+\theta_1) - \sin\Omega_1 \cdot \cos i_1 \cdot \sin(\omega_1+\theta_1)] \\ R_1 \cdot [\sin\Omega_1 \cdot \cos(\omega_1+\theta_1) + \cos\Omega_1 \cdot \cos i_1 \cdot \sin(\omega_1+\theta_1)] \\ R_1 \cdot \sin i_1 \cdot \sin(\omega_1+\theta_1) \end{pmatrix}. \tag{7}$$

The position vector of the second impulse is expressed by

$$\boldsymbol{R_2} = \begin{pmatrix} a_{geo} \cdot \cos\alpha_2 \\ a_{geo} \cdot \sin\alpha_2 \\ 0 \end{pmatrix} \tag{8}$$

and the pole vector defining the transfer orbit plane is

$$\boldsymbol{w} = \boldsymbol{R_1} \times \boldsymbol{R_2} \,/\, \| \boldsymbol{R_1} \times \boldsymbol{R_2} \| . \tag{9}$$

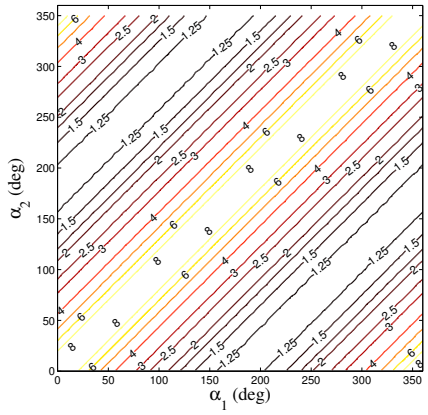


**Figure 3: Contour-map of the impulse function $\Delta V_{tot}$ (km/s) necessary to reach GEO. Initial orbit $O_1$: $p_1$= 22000 km, $e_1 = 0°$, $i_1$= 0°, $\Omega_1 = 0°$, $\omega_1 = 0°$.**

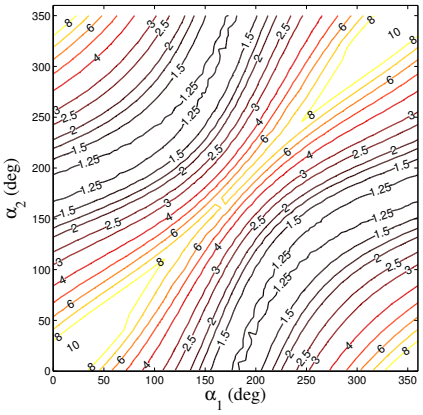


**Figure 4: Contour-map of impulse function $\Delta V_{tot}$ (km/s) necessary to reach GEO. Initial orbit $O_1$: $p_1$= 22000 km, $e_1 = 0.25°$, $i_1$= 0°, $\Omega_1 = 0°$, $\omega_1 = 0°$.**

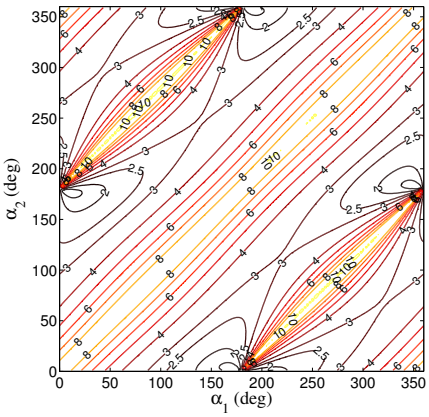


**Figure 5: Contour-map of impulse function $\Delta V_{tot}$ (km/s) necessary to reach GEO. Initial orbit $O_1$: $p_1$= 22000 km, $e_1 = 0°$, $i_1$= 20°, $\Omega_1 = 0°$, $\omega_1 = 0°$.**

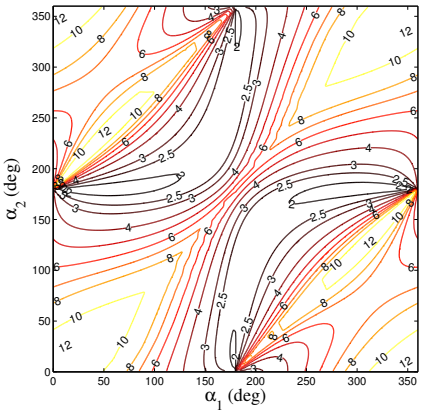


**Figure 6: Contour-map of impulse function $\Delta V_{tot}$ (km/s) necessary to reach GEO. Initial orbit $O_1$: $p_1$= 22000 km, $e_1 = 0.5°$, $i_1$= 25°, $\Omega_1 = 0°$, $\omega_1 = 0°$.**

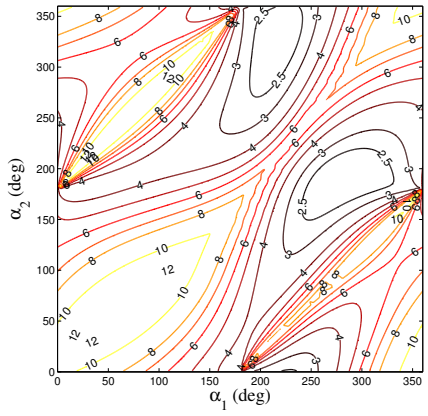


**Figure 7: Contour-map of impulse function $\Delta V_{tot}$ (km/s) necessary to reach GEO. Initial orbit $O_1$: $p_1$= 22000 km, $e_1 = 0.5°$, $i_1$= 25°, $\Omega_1 = 0°$, $\omega_1 = 60°$.**

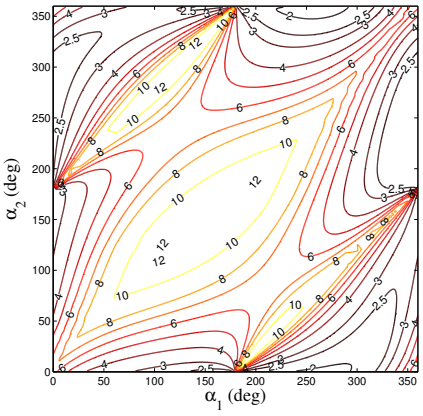


**Figure 8: Contour-map of impulse function $\Delta V_{tot}$ (km/s) necessary to reach GEO. Initial orbit $O_1$: $p_1$= 22000 km, $e_1 = 0.5°$, $i_1$= 25°, $\Omega_1 = 0°$, $\omega_1 = 150°$.**

The inclination $i_t$ and the right ascension of the ascending node $\Omega_t$ of the transfer orbit are then

$$i_t = \tan^{-1}\left( \frac{\sqrt{w_x^2 + w_y^2}}{w_z^2} \right)$$

$$\Omega_t = \tan^{-1}\left( \frac{w_x}{-w_y} \right) \tag{10}$$

and the transfer angle $\Delta$ is obtained by

$$\Delta = \cos^{-1}(\boldsymbol{R_1}/R_1 \cdot \boldsymbol{R_2}/R_2) \, . \tag{11}$$

Finally, the true anomalies of the impulses in the transfer orbit are given by the equations

$$f_1 = \tan^{-1}\left( \cot\Delta - \frac{R_1[p_t - R_2]}{R_2[p_t - R_1]\sin\Delta} \right)$$

$$f_2 = \tan^{-1}\left( -\cot\Delta + \frac{R_2[p_t - R_1]}{R_1[p_t - R_2]\sin\Delta} \right) \tag{12}$$

and the argument of perigee is either $\omega_t = -f_2$ if the intersection with *GEO* is at an ascending node, or $\omega_t = \pi - f_2$ if the intersection with *GEO* is at a descending node. The transfer orbit eccentricity is then

$$e_t = \frac{R_2 - R_1}{R_1 \cos f_1 - R_2 \cos f_2} \, . \tag{13}$$

The remaining parameter $a_t = p_t / (1 - e_t^2)$ is now readily available and we obtain a formulation of the impulse function of Eq. (4) with respect to the unknowns $\boldsymbol{X}$. In particular, we have (see e.g., **[9]**)

$$\boldsymbol{\Delta V_1} = \begin{pmatrix} \sqrt{\mu}\left( \frac{e_t}{\sqrt{p_t}} \sin f_1 - \frac{e_1}{\sqrt{p_1}} \sin\theta_1 \right) \\ \frac{\sqrt{\mu}}{R_1}\left( \sqrt{p_t} - \sqrt{p_1}\cos[i_t - i_1] \right) \\ \frac{\sqrt{\mu p_1}}{R_1} \sin[i_t - i_1] \end{pmatrix} \tag{14}$$

and

$$\boldsymbol{\Delta V_2} = \begin{pmatrix} \sqrt{\mu}\left( -\frac{e_t}{\sqrt{p_t}} \sin f_2 \right) \\ \frac{\sqrt{\mu}}{a_{geo}}\left( \sqrt{a_{geo}}\cos[i_2 - i_t] - \sqrt{p_t} \right) \\ \frac{\sqrt{\mu}}{\sqrt{a_{geo}}} \sin[i_2 - i_t] \end{pmatrix} . \tag{15}$$

An initial guess $\boldsymbol{X_{init}}(\theta_{1\,init}, \alpha_{2\,init}, p_{t\,init})$ being provided, we now search for a minimum of the impulse function given by Eqs. (4), (14) and (15). Different values of $\theta_{1\,init}$ and $\alpha_{2\,init}$ are used, spread over a mesh encompassing values between 0° and 360°. We also constrain $p_{t\,init}$ to stay within the prescribed bounds for an elliptical transfer orbit (**[2]**)

$$p_{t_{\min}} = \frac{R_1 R_2 - \boldsymbol{R_1} \cdot \boldsymbol{R_2}}{R_1 + R_2 + (\,2\,[R_1 R_2 + \boldsymbol{R_1} \cdot \boldsymbol{R_2}\,])^{1/2}},$$
$$p_{t_{\max}} = \frac{R_1 R_2 - \boldsymbol{R_1} \cdot \boldsymbol{R_2}}{R_1 + R_2 - (\,2\,[R_1 R_2 + \boldsymbol{R_1} \cdot \boldsymbol{R_2}\,])^{1/2}}, \tag{16}$$

and do not consider the case of hyperbolic transfer orbits. We use a quasi-Newton algorithm for finding local minima, as proposed by **[15].** The practical implementation is performed by invoking the NAG minimization routine E04JYF (**[16]**). If the obtained minimum underbids a given user-supplied threshold (in terms of km/s) then the corresponding transfer orbit $O_t$ and the thrust vectors $\boldsymbol{\Delta V_j}$ ($j$ = 1, 2) are retained. The solution is then subjected to further operational consistency tests, presented in Section III.2. In the successful case the transfer is finally accepted as a potential mission recovery scenario.

*III.1.3 Solution of the switching equations*

The Lawden 'primer vector' formalism (**[1], [9]**) allows to express the conditions for an optimal bi-impulsive transfer between a pair of elliptical orbits in the form of a set of 3 nonlinear algebraic equations,

$$\begin{cases} (1+q_1)J_1 - q_1 T_1 = (1+q_2)J_2 - q_2 T_2 \\ (y_1 T_1 - q_1 S_1)(T_1 - J_1) - S_1 T_1 + y_1 W_1^2 + K_1 W_1 = 0 \\ (y_2 T_2 - q_2 S_2)(T_2 - J_2) - S_2 T_2 + y_2 W_2^2 + K_2 W_2 = 0 \quad . \end{cases} \tag{17}$$

where

$$\begin{aligned} & x_j = e_t \cos f_j, \quad \mathrm{y_j} = e_t \sin f_j, \quad q_j = 1 + e_t \cos f_j, \quad j = 1,\ 2 \\ & J_1 = (S_2 - S_1 \cos\Delta)/\sin\Delta \\ & J_2 = (S_2 \cos\Delta - S_1)/\sin\Delta \\ & K_1 = (q_2 W_2 - q_1 W_1 \cos\Delta)/\sin\Delta \\ & K_2 = (q_2 W_2 \cos\Delta - q_1 W_1)/\sin\Delta\,. \end{aligned} \tag{18}$$

The switching equations of Eq. (17) provide an analytical means for the optimization of the unknown vector $\boldsymbol{X}(\theta_1, \alpha_2, p_t)$. The primer vector

$$\boldsymbol{P_j} = \begin{pmatrix} S_j \\ T_j \\ W_j \end{pmatrix} \qquad j = 1,\ 2 \tag{19}$$

is the unit vector in the direction of the thrust and satisfies

$$\boldsymbol{P_j}\,|\boldsymbol{\Delta V_j}| = \boldsymbol{\Delta V_j}, \quad j = 1, 2 \tag{20}$$
$$S_j^2 + T_j^2 + W_j^2 = 1\ , \quad j = 1, 2. \tag{21}$$

An optimal solution to Eq. (17) must also satisfy the additional conditions (see Equations (8) and (11) in **[9]**)

$$q_1 T_1 \geq q_2 T_2 \quad (22)$$
$$S_1^2 + J_1^2 = S_2^2 + J_2^2 \leq 0.25. \quad (23)$$

The first condition of Eq. (22) checks for the correct sequence of the impulses i.e. guarantees the first impulse to precede the second one. Equation (23) constrains the elevation angle of the optimal impulses to be less than 30° from the local horizontal plane. We solve Eqs. (17) by using the Powell hybrid method for the root finding of a set of nonlinear equations (**[17]**). The practical implementation is performed by the NAG routine C05NDF (**[16]**). Once more, the solution transfer orbit $O_t$ and the thrust vectors $\Delta \mathbf{V}_j$ ($j$ = 1, 2) are retained and subjected to further operational consistency tests as presented in Section III.2.

### III.2 Step 2: Practical recovery mission design

The results from Step 1 are used to develop a complete mission recovery design including multiple finite-thrust burns as well as third-body perturbations. This is done by using the mission design and optimization software PANTHEON (**[13]**).
Realistic *LAE* thrust values and burn duration constraints generally call for several *LAE* maneuvers, typically 4 or more. The transition from the two instantaneous infinite-thrust impulses used in Step 1 to the case of multiple *LAE* burns requires an additional optimization of the burn parameters. For instance, the burn locations (in terms of their right ascensions and longitudes) need to be readjusted and the exact duration of each *LAE* ignition needs to be computed. This optimization is performed as described in §5 of **[13]**.
The PANTHEON software then numerically propagates the satellite from the non-nominal injection orbit $O_1$ to *GEO*. This propagation is performed by using a Runge-Kutta-Nystroem scheme as described in **[13]** and **[18]**. In contrast to the Keplerian motion assumed in Step 1, the orbit is now accurately modeled, taking into account for following perturbations: J2 and J4 coefficients of the Earth's gravitational potential, Earth's precession and nutation, the gravitational influence of the Sun and the Moon and solar radiation pressure. Finally, the software also considers additional mission operational constraints such as e.g.:

- the requirement of ground station visibility at the instants of each *LAE* burn ignition
- the necessity to avoid interferences with other operating geostationary satellites, generated by the use of the same frequency band for commanding, telemetry and payload
- various constraints on spacecraft attitude

## IV Case Study: Premature Abort of the Second Burn of a Re-ignitable Upper Rocket Stage Engine

The approach developed in Section III is illustrated by simulating a realistic transfer orbit mission contingency scenario. We start from the assumption that, at the beginning, a standard geosynchronous transfer orbit strategy has been targeted. The launch is performed from Kennedy Space Center, Fl, USA. We use three ground stations for permanent visibility of the spacecraft: Luxembourg 1 (L1), Australia 1 (A1) and South America 1 (SA1). The nominal injection parameters after the successful completion of the upper rocket stage second burn are shown in Table 1 and an illustration of the situation is depicted in the scheme of Fig. 9.

**Table 1: Consequences on the injection orbit $O_1$ of a 60 s premature abort of the upper rocket stage engine. The simulated injection GMT time is 2007/04/28, 4:28:10.**

| | $a_1$ (km) | $e_1$ (deg) | $i_1$ (deg) | $\Omega_1$ (deg) | $\omega_1$ (deg) | $v_1$ (deg) |
|---|---|---|---|---|---|---|
| nominal mission | 27375.558 | 0.540 | 23.972 | 9.006 | 180.003 | 180.064 |
| 60 s premature upper stage abort | 19720.320 | 0.572 | 25.039 | 2.244 | 150.823 | 144.248 |

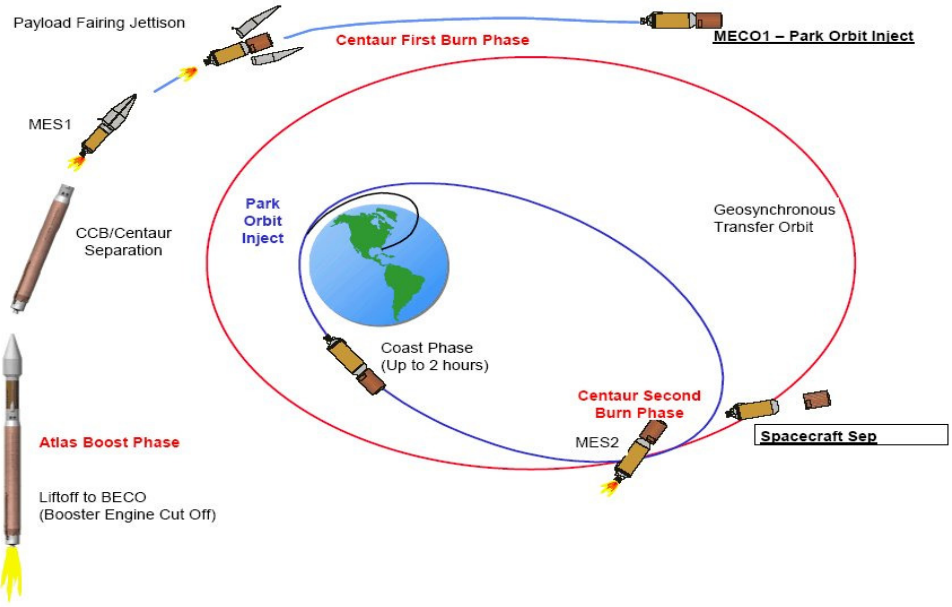


**Figure 9: GTO injection of a spacecraft by a re-ignitable upper rocket stage engine (courtesy: Atlas Launch System Mission's Planner's Guide, 1998, ILS International Launch Services Inc. and Lockheed Martin Corporation)**

We now simulate the case of a 60 s premature abort of the second burn of the upper stage of the rocket. The impact on injection orbit parameters is shown in Table 1. The semi-major axis $a_1$ is about 30% lower than in the nominal situation and the inclination $i_1$ is larger by about 1°. In addition, a considerable node shift of about 30° is introduced by the failure of the rocket.
In what follows, we analyze the possibility of a mission recovery with the on-board fuel of the satellite. This is done by applying our two steps methodology. In Section IV.1 we study the outcome of the Step 1 techniques described in Section III.1 and test these solutions against some first mission operational constraints. Step 2 is then applied in Section IV.2 to obtain a realistic recovery design for the 60 s upper stage shortage by taking into account multiple finite-thrust burns, third-body orbital perturbations as well as various additional operational constraints. Section IV.3 gives supplementary results.

### IV.1 Selection of the recovery strategy

Figure 10 shows the p-optimized contour plots and the solution of the switching equations for the non-nominal injection orbit $O_1$ shown in Table 1. The four solutions to Eqs. (17) are shown by circular, square, triangular and diamond markers, respectively. Every solution satisfies a consistency test propagation to *GEO*. This test propagation consists of two infinite-thrust impulses applied in a Keplerian gravitational potential, at the right ascensions indicated by Fig. 10. The conditions for acceptance of the test propagation are such that the final orbit semi-major axis $a_2$ be in the interval [42050:42300] km and that $e_2 < 0.05°$ and $i_2 < 0.5°$.
We identify two solutions of the switching equations that coincide with the location of the deepest valleys of the impulse function as obtained by the p-optimization method. They can be found in the lower left quadrant of Fig. 10 at $(\alpha_1, \alpha_2, p_t)$ = (-93.75°, -2.35°, 16506.920 km) and $(\alpha_1, \alpha_2, p_t)$ = (-12.32° ,-133.75°, 32815.721 km). The propellant expenditure is $\Delta V_{tot}$ = 2.107 km/s and $\Delta V_{tot}$ = 2.292 km/s, respectively. For these two solutions, the optimality conditions of Eqs. (22) and (23) are fulfilled, whereas the remaining two solutions in the upper right quadrant do not verify these equations.
The different markers for each of the four points are used to indicate whether several operational constraints on the satellite are fulfilled at the instant of the burns and whether the transfer is of 'short' or 'long' type. At the impulsive ignitions $j$ ($j$ = 1, 2) of the satellite's liquid apogee engine (hereafter *LAE*) thermal, power and sensor constraints are such that the angle $\phi_j$ between the spin axis of the spacecraft and the Sun needs to stay within a prescribed interval $[\phi_{j\,min}, \phi_{j\,max}]$. We use the values $\phi_{j\,min}$ =

50° and $\phi_{j\ max}$ = *100°*. The circular and square markers indicate the transfers where both $\phi_j$ lie in this interval. A short transfer has a transfer angle $\Delta < 180°$ and for a long transfer $\Delta > 180°$.

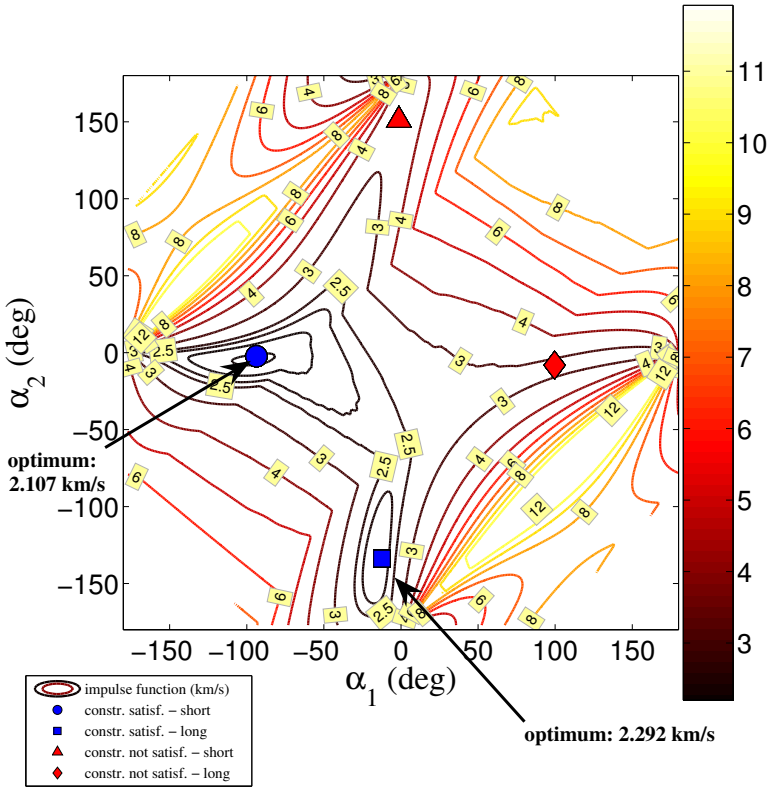


**Figure 10: Simulation of a 60 s premature breakdown of the second burn of a re-ignitable upper rocket stage engine. Contour-map of the impulse function $\Delta V_{tot}$ to reach GEO and switching equations solution. The right ascensions $\alpha_1$ and $\alpha_2$ indicate the location of the two infinite-thrust impulses in inertial space.**

Figure 11 shows the same plot but for the results of the minimization method. We observe a broad agreement between the solutions of the switching equations of Fig. 10 and the outcome of the numerical impulse function minimization of Fig. 11. A number of minima can be found around the locations of the four solutions of the switching equations. In the valleys (-93.75°, -2.35°) and (-12.32° ,-133.75°) the data points are densely congested but do not coincide. We explain this finding by the long and narrow shape of these valleys, possibly containing several distinct minima. Numerical artifacts of the minimization method may also be at the origin of the scattering of the results in these regions. Apart from the minima close to the solutions of the switching equations we also obtain additional results. For example, the isolated minimum at (2.24°,-177.76°) has $\Delta V_{tot}$ = 2.842 km/s. The numerical minimization of the impulse function provides thus complementary information to the switching equations outcome. The legend to Fig. 11 is similar to the one of Fig. 10.

### IV.2 Practical mission recovery

We use the minimum-fuel solution obtained in IV.1 that satisfies the constraints on the sun aspect angles $\phi_j$ , i.e. the optimum of $\Delta V_{tot}$ = 2.107 km/s at ($\alpha_1$, $\alpha_2$, $p_t$) = (-93.75°, -2.35°, 16506.920 km). Step 2 of the method (see Section III.2) is now applied to develop a complete mission recovery scenario including multiple finite-thrust burns as well as third-body perturbations. We consider a model satellite with a re-ignitable on-board engine using liquid bipropellant. The specifications of our spacecraft are shown in Table 2. Our final mission recovery design to *GEO* comprises 7 burns and is summarized in Table 3 and illustrated by Fig. 12.

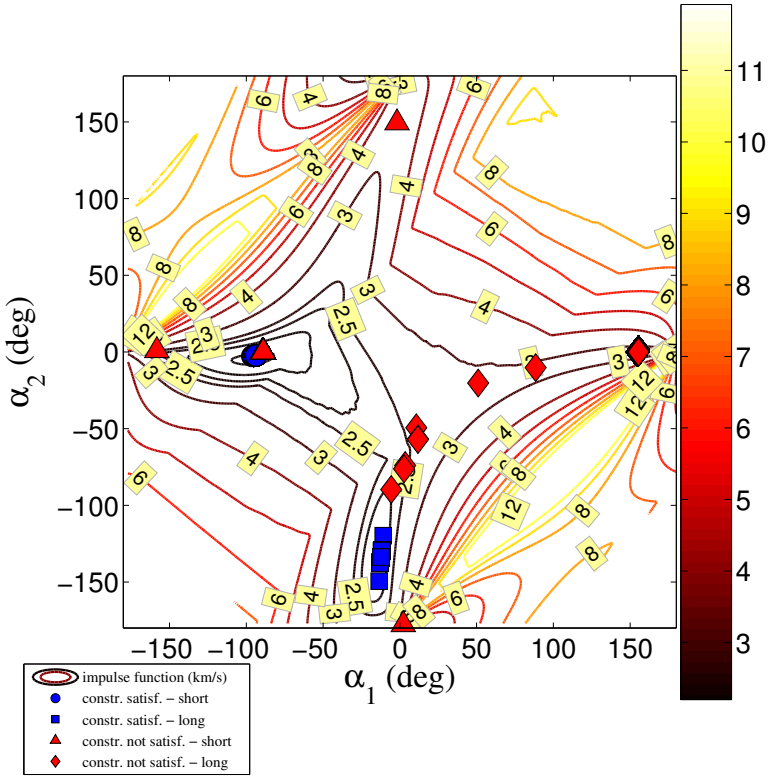


**Figure 11: : Simulation of a 60 s premature breakdown of the second burn of a re-ignitable upper rocket stage engine. Contour-map of the impulse function $\Delta V_{tot}$ to reach GEO and corresponding local minima. The right ascensions $\alpha_1$ and $\alpha_2$ indicate the location of the two infinite-thrust impulses in inertial space.**

**Table 2: Specifications for the model satellite used for the mission recovery**

| $I_{sp}$ (s) | $F$ (N) | Initial wet mass (kg) | Mass flow rate (kg/s) | Maximum burn duration (s) |
|---|---|---|---|---|
| 320 | 450 | 4250 | 0.15 | 3000 |
| **Nominal GTO $\Delta V_{tot}$ (km/s)** | **Nominal in-orbit lifetime (yrs)** | **Consumption for GEO stationkeeping manoeuvers (km/s /yr)** | **Consumption in inclined orbit (km/s /yr)** | **Total propellant aboard (km/s)** |
| 1.444 | 15 | 0.05 | 0.0025 | 1.444 + (15·0.05) ≈ 2.2 |

### IV.3 Overall results

In Fig. 13 we show the total propellant expenditure $\Delta V_{tot}$ of the recovery as a function of the burn shortage of the upper stage. For comparison we also plot the $\Delta V$ necessary for the nominal *GTO* mission (1.444 km/s, see Table 2) plus the $\Delta V$ the upper stage was not able to consume due to the abort. The total propellant aboard our model satellite is about 2.2 km/s (see Table 2). A 60 s premature abort of the upper rocket stage, as described in Sections IV.2 and IV.3, produces thus an injection orbit on the limit of being recoverable by our model satellite.

Figure 14 shows the remaining satellite lifetime after a successful recovery as a function of the upper stage burn shortage. The lower line (in green) indicates the lifetime left on *GEO* assuming that a year of North-South and East-West stationkeeping maneuvers consume about 0.05 km/s (Table 2). The upper line (in orange) indicates the remaining spacecraft lifetime in inclined orbit i.e. in the case where

**Table 3: Mission recovery strategy for the 60 s premature breakdown of an upper stage rocket engine. Each row shows the transfer orbit parameters obtained after performing burn *n* (*n* = 1,…,7). The first column holds the components of the thrust vector in the Earth-centered inertial coordinate system. The total propellant $\Delta V_{tot}$ used is approximately 2.107 km/s.**

| Orbit (and approximate $\Delta V_{xyz}$ [km/s]) | Epoch yr/mth/day hr:min:sec | a (km) | e (deg) | i (deg) | Ω (deg) | ω (deg) | ν (deg) | *LAE* burn duration (s) |
|---|---|---|---|---|---|---|---|---|
| *injection orbit* | 2007/04/21 4:28:10 | 19720.320 | 0.572 | 25.039 | 2.244 | 150.825 | 144.248 | / |
| *after burn #1* (0.293, -0.146, 0.016) | 2007/04/21 9:42:49 | 23287.850 | 0.589 | 25.069 | 359.572 | 165.463 | 69.357 | 3000.0 |
| *after burn #2* (0.182, -0.085, 0.035) | 2007/04/21 19:28:21 | 26458.850 | 0.616 | 24.944 | 357.723 | 174.389 | 61.406 | 1753.7 |
| *after burn #3* (0..102, 0.377, -0.229) | 2007/04/22 1:16:43 | 28487.898 | 0.495 | 15.286 | 356.687 | 174.854 | 261.962 | 3000.0 |
| *after burn #4* (0.022, 0.088, -0.053) | 2007/04/23 3:55:30 | 29164.159 | 0.461 | 13.358 | 356.524 | 175.148 | 354.380 | 744.0 |
| *after burn #5* (0.077, 0.301, -0.184) | 2007/04/24 7:13:41 | 32110.017 | 0.324 | 7.661 | 356.274 | 175.367 | 201.640 | 2344.3 |
| *after burn #6* (0.102, 0.407, -0.249) | 2007/04/25 14:58:15 | 38688.268 | 0.098 | 1.719 | 354.590 | 177.197 | 333.804 | 2735.4 |
| *after burn #7* (0.034, 0.142, -0.087) | 2007/04/27 9:18:51 | 42164.170 | 0.006 | 0.058 | 280.825 | 256.1344 | 40.943 | 851.8 |

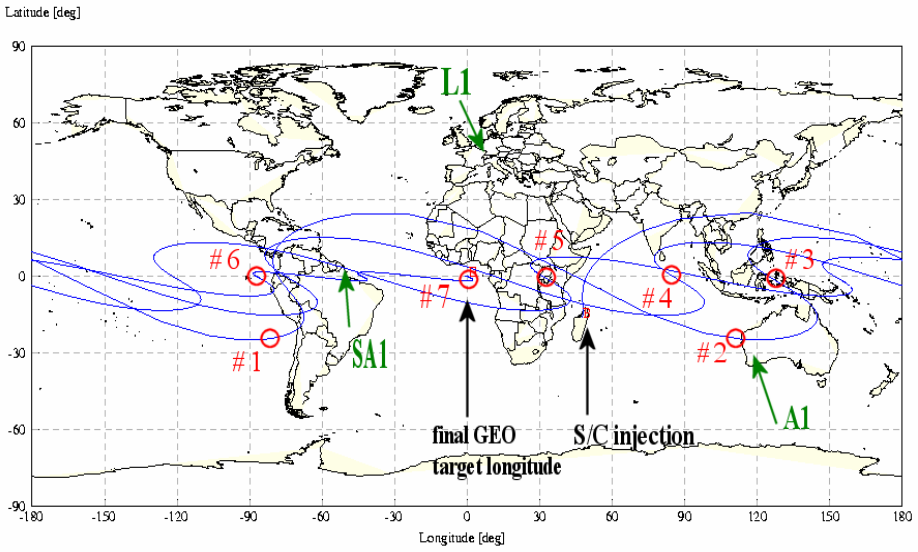


**Figure 12: Practical mission recovery for the 60 s premature breakdown of an upper rocket stage engine. The circles (in red) indicate the longitude and latitude of burn *n* (*n* = 1,…,7) (see also Table 3). The arrows (in green) mark the longitude and latitude of the used ground stations.**

inclination control is not performed any more. The dashed lines show a linear interpolation between the data point at 60 s and the limit value of about 77 s, for which the satellite is not recoverable any more with its on-board fuel. We note that for an upper stage abort of half a minute, our model satellite can still spend about half of its nominal lifetime on *GEO*. For a 1 minute premature abort, the satellite is capable to spend more than 30 yrs in inclined orbit. In the case of a 1.5 minutes abort, the satellite is not capable to reach *GEO* with its on-board propellant (see hashed zone [in red] on Fig. 14).

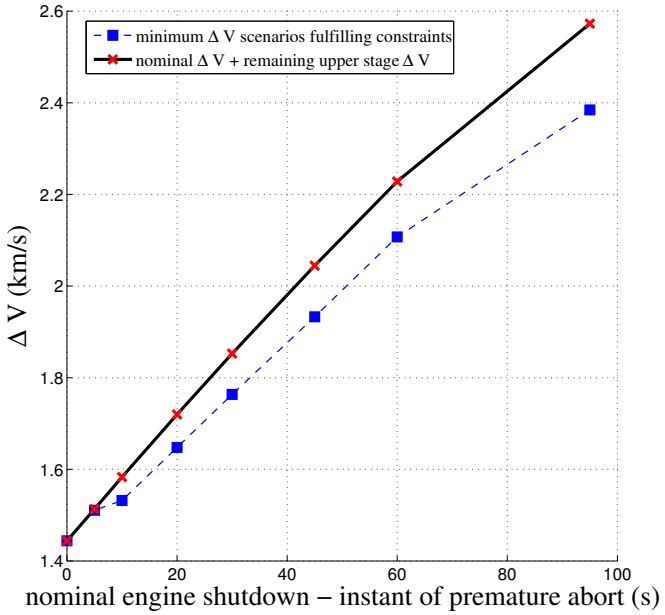


**Figure 13: Dashed (line in blue): total velocity increment $\Delta V_{tot}$ needed to reach *GEO* vs upper stage second burn shortage. Solid line: $\Delta V$ necessary for the nominal *GTO* mission plus the $\Delta V$ the upper stage was not able to consume due to the abort.**

## V Conclusion

We analyzed the possibility to save a geostationary transfer orbit mission in distress with the on-board propellant of the spacecraft. As part of our methodology, we searched first for recovery simplified scenarios by implementing three different methods, originally developed in the limit of two infinite-thrust impulses applied in a Keplerian gravitational potential: (1) p-optimized impulse function contouring, (2) numerical minimization of the impulse function and (3) the solution of the switching equations. We show these methods to be applicable in realistic *GTO* contingency cases and to provide an initial guess for a practical design of the recovery (Figs. 10-11). This practical design takes into account for multiple finite-thrust burns of the satellite's *LAE*, third-body orbital perturbations and various mission operational constraints such as e.g., Sun aspect angles or ground station visibility (Fig. 12).

We validated the approach by presenting a test case where we studied the possibility to recover from a premature abort of the second burn of a re-ignitable upper rocket stage engine. We determined the remaining satellite lifetime on *GEO* after successful recovery as a function of the burn shortage of the launch vehicle (Fig. 14). We also addressed the question of potentially re-designing the entire mission

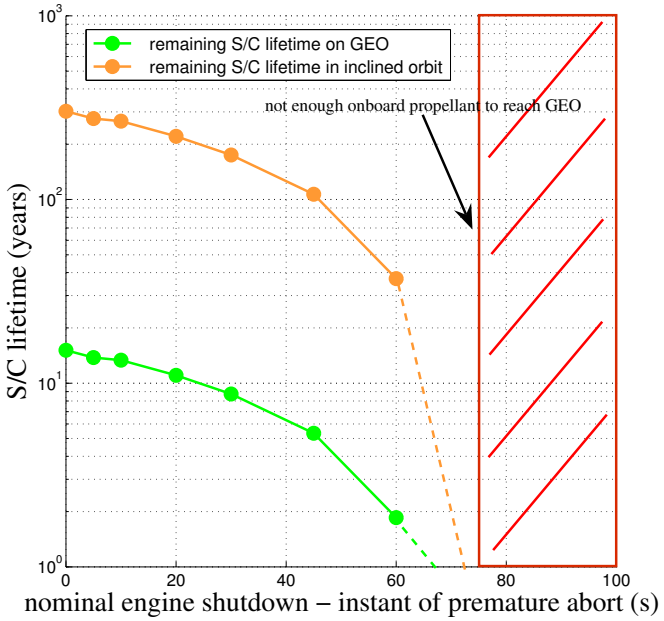


**Figure 14: Remaining satellite lifetime vs upper stage second burn shortage. The lower line (in green) shows the remaining lifetime on *GEO* assuming a nominal lifetime of 15 years and a consumption of 0.05 km/s per year for stationkeeping maneuvers (see also Table 2). The upper line in orange indicates the remaining lifetime assuming that the spacecraft is put on inclined orbit immediately after recovery i.e. no North-South stationkeeping is performed. The hashed zone in red shows the region where the mission is not recoverable with the on-board propellant of the spacecraft.**

after the successful recovery by computing the lifetime of the satellite in inclined orbit, i.e. in the case where inclination control is not performed any more. This option may be of particular interest in the case where the remaining *GEO* lifetime is small e.g., less than 1 yr. In these conditions, the lifetime in inclined orbit is still considerable for our model satellite (> 30 yrs). Finally, we also identify the regime where no recovery is possible with the on-board fuel of the spacecraft (hashed zone on Fig. 14). In this case, alternate recovery strategies must be considered or the spacecraft must be de-orbited.

Further *GTO* contingency cases were analyzed, but not shown in this work for the sake of conciseness. We simulated the non-nominal behavior of several re-ignitable and non re-ignitable launch vehicles and computed again the minimum propellant needed for a recovery. For more than 95% of the studied injection orbits, our three methods converged to results much alike the ones shown in Section IV.2 (Figs. 10 and 11). Although the magnitudes of the isocontours and the minimum velocity increment $\Delta V_{tot}$ needed to perform the transfer varied from case to case (depending on the actual injection orbit parameters), the switching equations solutions and the numerical minimization approach converged to the same transfer orbits. In some cases however, no elliptical transfer orbit could be obtained that verified the switching equations and the optimality conditions of Eqs. (22) and (23). Some minima retrieved by the numerical impulse function minimization, on the other hand, were found to be located as usual within the contour valleys. These cases showed the importance of implementing the three complementary techniques to search for elliptical transfer orbits. Finally, the subsequent design of a realizable recovery scenario as shown in IV.3 (Table 3 and Fig. 12) ultimately depends on the amount of propellant aboard the spacecraft and on the nature and the severity of the hazard encountered during launch.

## Acknowledgments

The first author would like to thank Markus Gross for his helpful comments. The work was supported by grant BFR 04/55 of the Ministry for Higher Education and Research, Grand-Duchy of Luxembourg.

## References

**[1]** Lawden, D.F., Optimal Trajectories for Space Navigation, 1st ed., Butterworth Mathematical Texts, Butterworths, London, 1963

**[2]** McCue, G.A., Optimum Two-Impulse Orbital Transfer and Rendezvous between Inclined Elliptical Orbits, 1963, AIAA Journal, Vol. 1, No. 8, pp. 1865-1872

**[3]** Lee, C., An Analysis of Two-Impulse Orbital Transfer, 1964, AIAA Journal, Vol. 2, No. 10, pp. 1767-1773

**[4]** McCue, G.A., Bender, D.F., Numerical Investigation of Minimum Impulse Orbital Transfer, 1965, AIAA Journal, Vol. 3, No. 12, pp. 2328-2334

**[5]** Jezewski, D.J., Rozendaal, H.L., An Efficient Method for Calculating Optimal Free-Space N-Impulse Trajectories, 1968, AIAA Journal, Vol. 6, No. 11, pp. 2160-2165

**[6]** Marchal, C., Une Expression des Commutations sous Forme Explicite dans le Problème des Transferts Optimaux entre orbites Keplériennes, Rech. Aerosp., Vol. 11, No. 10/11, 1984, pp. 621-631.

**[7]** Jezewski, D.J., Mittleman, D., An Analytic Approach to Two-Fixed-Impulse Transfers Between Keplerian Orbits, 1982, J. Guidance, Vol. 5, No. 5, pp. 458-464

**[8]** Eckel, K.G., Vinh, N.X, Optimal Switching Conditions for Minimum Fuel Fixed Time Transfer between Non-Coplanar Elliptical Orbits, Acta Astronautica, Vol. 11, No. 10/11, 1984, pp. 621-631

**[9]** Vinh, N.X., Kuo, S.H., Marchal, C., Optimal Time-Free Nodal Transfers between Elliptical Orbits, Acta Astronautica, Vol. 17, No. 8, 1988, pp. 875-880

**[10]** Abdelkhalik, O., Orbit Design and Estimation for Surveillance Missions using Genetic Algorithms, 2005, Ph.D thesis, Texas A&M University

**[11]** Abdelkhalik, O., Mortari, D., N-Impulse Orbit Transfer Using Genetic Algorithms, 2007, J. of Spacecraft and Rockets, Vol. 44, No. 2, pp. 456-459

**[12]** Cazala-Hourcade, E., Marcille, N., Fast Optimisation of Apogee Manoeuvres on Geostationary Orbits, 1992, Proceedings of the "43rd Congress of the International Astronautical Federation", Washington DC, IAF-92-0019

**[13]** Francken, P., Laroche H., Methods for the Design and Optimisation of Complex Transfer Orbit Missions, 1995, Proceedings of the "International Symposium on Spaceflight Dynamics", Toulouse, Ed. Cepaduès, pp. 493-502

**[14]** Battin, R.H. , An Introduction to the Mathematics and the Methods of Astrodynamics, Revised Edition, AIAA Education Series, 1987

**[15]** Gill, P.E., Murray, W., 1976, Minimization Subject to Bounds on the Variables, NPL Report NAC 72, National Physical Laboratory

**[16]** NAG Fortran 90 Library Manual, Mark 20, The Numerical Algorithms Group

**[17]** Powell, M.J.D., 1970, A Hybrid Method for Nonlinear Algebraic Equations, Numerical Methods for Nonlinear Algebraic equations, ed. P. Rabinowitz, Gordon and Breach

**[18]** Filippi, S., Graef, J., 1986, J. Comp. Appl. Math., Vol. 14, pp. 361-370